Dynamo action by turbulence in absolute equilibrium

SRINIVASA GOPALAKRISHNAN GANGA PRASATH, STÉPHAN FAUVE and MARC BRACHET

Laboratoire de Physique Statistique, Ecole Normale Supérieure, CNRS, Université P. et M. Curie,
Université Paris Diderot - Paris, France

Abstract – We consider the generation of a large-scale magnetic field by a turbulent flow driven by a small-scale helical forcing in a low magnetic Prandtl number fluid. We provide an estimate of the dynamo threshold that takes into account the presence of large-scale turbulent fluctuations by considering that the scales of the flow that mostly contribute to the dynamo process are roughly in absolute equilibrium. We show that turbulent flows in absolute equilibrium do generate dynamos and we compare their growth rates to their laminar counterparts. Finally, we show that the back reaction of the growing magnetic field modifies the statistical properties of turbulent flow by suppressing its kinetic helicity at large magnetic Reynolds number.

Introduction. – Magnetic fields of planets and stars are believed to be generated by a dynamo process, an instability that results from electromagnetic induction by the flow of an electrically conducting fluid [1]. Small perturbations of a magnetic field are amplified provided the magnetic Reynolds number, R_m^I, is large enough. $R_m^I = \mu_0 \sigma V l$, where μ_0 is the magnetic permeability of vacuum, σ is the electrical conductivity, V is the order of magnitude of the velocity and l is the characteristic (integral) length scale of the flow. An important property of liquid metals as well as of stellar plasmas is the extremely small value of their magnetic Prandtl number, $P_m = \mu_0 \sigma \nu < 10^{-5}$, where ν is the kinematic viscosity. Thus, the kinetic Reynolds number of the flow, $Re^I = R_m^I / P_m$ becomes huge when R_m^I is increased to reach a dynamo regime and the flow displays strong turbulent fluctuations. The effect of these fluctuations on the efficiency of the amplification mechanism of the magnetic field as well as on its saturation by the Lorentz force above the dynamo threshold is to a large extent an open problem. Direct numerical simulations are not possible in the parameter range of experiments in liquid metal but they have displayed the following trend for larger values of P_m: for a flow forcing with a given geometry, the dynamo threshold first increases and then saturates when the magnetic Prandtl number is decreased. This has been observed with the Taylor-Green flow [2], with a von-Karman–type forcing [3] and with the Arnold-Beltrami-Childress (ABC) flow [4]. For low P_m, *i.e.* small kinematic viscosity compared to magnetic diffusivity, the forced flow

undergoes hydrodynamic instabilities before reaching the dynamo threshold, thus the increase in dynamo threshold has been often related to the inhibition of dynamo mechanisms by turbulent fluctuations. Note, however, that a similar increase of threshold when P_m is decreased has been observed when the flow is generated by a random forcing [5]. All the deterministic forcings quoted above have been simulated in the absence of scale separation, *i.e.* the magnetic field cannot grow at a scale larger than the integral scale of the flow. A more recent study has been performed with a moderate scale separation using an ABC forcing at a scale smaller than the one of the first Fourier mode of the simulation. It has been reported that the increase in dynamo threshold, between the one of the laminar flow at large P_m and its saturation value when P_m is small enough, is smaller than for simulations that do not involve scale separation [6]. Slightly above the dynamo threshold, ABC flows or more generally flows with strong kinetic helicity, are expected to generate a magnetic field at large scales through the alpha effect [1]. It is not known whether the dynamo threshold dependence on P_m becomes weaker and weaker for these flows when the scale separation is increased. Indeed, direct numerical simulations cannot both handle a wide scale separation between the large-scale magnetic field and the spatial periodicity of the flow, and resolve the turbulent cascade above the forcing scale when P_m is small. We report here a new approach that can provide a way to study a dynamo generated by a helical flow with scale separation in the small P_m limit. The idea is to model the flow using the

truncated Euler equation. This is motivated by the observation that velocity fluctuations at scales larger than the forcing are in statistical equilibrium [7] when Re is large (equivalently P_m is small). A second crucial assumption is that the velocity field at scales smaller than the one of the forcing does not contribute to the generation of the large-scale magnetic field and thus can be discarded in the flow model. This relies on an observation provided by the Karlsruhe experiment [8] for which it has been shown that the correct value of the dynamo threshold is predicted when the small-scale turbulent fluctuations are not taken into account. Note that with our procedure only small-scale fluctuations are discarded, whereas large-scale fluctuations are taken into account.

This paper is organized as follows: in the next section, we recall the governing equations and the numerical method. We consider the dynamo generated by an ABC forcing at two different wave numbers in the third section. We show that the velocity field displays a large-scale spectrum roughly similar to the one of absolute equilibrium (AE). Despite these large-scale fluctuations, the dynamo threshold remains low, $R_m^c \sim 10$. After recalling the concept of AE in the fourth section, we show that these flows display dynamo action at low threshold provided they are helical enough and we compare their dynamo efficiency to that of the single-mode ABC dynamo at large P_m (fifth section). These results are analyzed using simple arguments in the sixth section. The Lorentz force back reaction effect on the flow is discussed in the seventh section. Finally, we conclude by proposing a new configuration of a dynamo experiment in which we can take advantage of helical forcing and scale separation in order to reach the dynamo threshold at reasonable values of R_m despite the presence of AE large-scale turbulent fluctuations.

Governing equations. – The equations of magneto-hydrodynamics (MHD) governing an incompressible velocity field $\boldsymbol{u}$ of a fluid with unit density and magnetic induction $\boldsymbol{b}$ (in units of Alfvèn velocity) read

$$\partial_t \boldsymbol{u} + (\boldsymbol{u} \cdot \nabla)\boldsymbol{u} = -\nabla p + \boldsymbol{j} \times \boldsymbol{b} + \nu \Delta \boldsymbol{u} + \boldsymbol{f}, \quad (1)$$

$$\partial_t \boldsymbol{b} = \nabla \times (\boldsymbol{u} \times \boldsymbol{b}) + \eta \Delta \boldsymbol{b}, \quad (2)$$

where $\boldsymbol{j}$ is the current density, $\boldsymbol{j} = \nabla \times \boldsymbol{b}$, and $\nabla \cdot \boldsymbol{u} = 0 = \nabla \cdot \boldsymbol{b}$. p is the pressure, $\boldsymbol{f}$ is the mechanical forcing, ν is the kinematic viscosity and $\eta = 1/\mu_0 \sigma$ is the magnetic diffusivity. They are solved numerically in a periodic domain of length 2π using the pseudo-spectral code GHOST [9]. This parallel solver uses a Runge-Kutta time-stepping method and FFTW. Dealiasing is done by the 2/3 rule [10], so that runs at resolution N^3 have maximum wave number $k_{\max} = N/3$.

The so-called ABC velocity field

$$\boldsymbol{u}_{\mathrm{ABC}}^{(k_0)}(x, y, z) = [B\cos(k_0 y) + C\sin(k_0 z)]\hat{x}$$
$$+ [C\cos(k_0 z) + A\sin(k_0 x)]\hat{y}$$
$$+ [A\cos(k_0 x) + B\sin(k_0 y)]\hat{z} \quad (3)$$
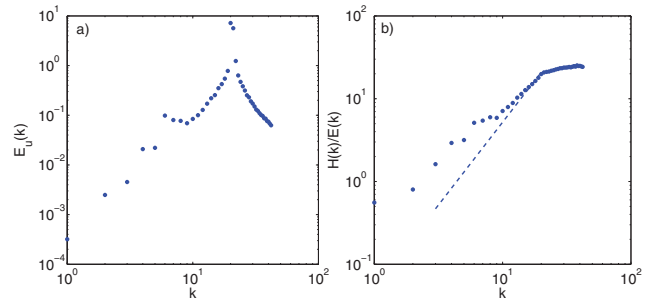
Fig. 1: (Colour on-line) (a) Kinetic energy $E_u(k)$ and (b) relative kinetic helicity $H(k)/E_u(k)$ spectra for ABC flow forced at $k_0 = 20$ and 21 with finite viscosity ($Re = 200$) and resolution 128^3. The dashed line represents k^2 indicating an AE-like behavior at large scales.

is a stationary solution to the Euler equation (1), with vanishing viscosity, forcing term and magnetic field. This field will be used below to build both initial conditions and the forcing term $\boldsymbol{f} = -\nu k_0^2 \boldsymbol{u}_{\mathrm{ABC}}^{(k_0)}$ needed to maintain the velocity field (for the ABC runs). Dynamo action is studied by using a small amplitude random magnetic initial data (that involves the smallest available wave numbers $k = k_{\mathrm{box}} = 1$) and monitoring the magnetic growth rates.

The standard ABC with $A = B = C = 1$ will be utilized in all simulations and its total kinetic energy is given by $E_u = \frac{\langle u^2 \rangle}{2} = \sum_{k=0}^{k_{\max}} E_u(k) = 3/2$. $E_u(k)$ denotes the kinetic energy spectrum. Similarly $E_b(k)$ denotes the magnetic energy spectrum and $H(k)$ the kinetic helicity spectrum. The large-scale kinetic and magnetic Reynolds numbers are defined, respectively, as $Re = \sqrt{2E_u}/k_{\mathrm{box}}\nu$ and $R_m = \sqrt{2E_u}/k_{\mathrm{box}}\eta$.

ABC forcing at 2 different wave numbers. – When P_m is large enough, the laminar flow $\boldsymbol{u}_{\mathrm{ABC}}^{(k_0)}$ driven by an ABC forcing remains stable up to the dynamo threshold. In order to get a first hint about the effect of velocity fluctuations on the dynamo threshold in a configuration that involves both an ABC-type forcing and scale separation at moderate Prandtl number, we consider a forcing term that is the sum of 2 ABC flows at $k_0 = 20$ and $k_0 = 21$. The viscosity in this special case is adjusted to produce the desired Re, and not a kinetic energy $E_u = 3/2$. Figure 1(a) demonstrates that this forcing generates velocity fluctuations. In addition, despite the moderate value of Re ($Re = 200$) their spectrum shows statistical equilibration at large scales. Indeed, at small wave numbers $k < 20$ the kinetic spectrum displays a range which roughly approximates energy equipartition $E(k) \sim k^2$. Although the data are rather scattered at low k, the behavior of the relative kinetic helicity shown in fig. 1(b) confirms that the large scales are in absolute equilibrium (see below eq. (4)). This type of equilibrium range is well known, in the non-helical case, to be fed by beating-type interactions between eddies in the energy-containing range, this being balanced by an eddy viscosity also coming mostly from the energy containing range [7].

Table 1: Critical R_m corresponding to ABC forcing at two wave numbers (both at $Re = 200$), AE velocity field and single-mode ABC velocity field.

Type	Resolution	ζ	Critical R_m
Forced: $k_0 = 20, 21$	128	–	10.16
Forced: $k_0 = 10, 11$	64	–	7.908
AE	64	1	10.35
AE	32	1	8.36
ABC	64	0.35	6.93
ABC	64	0.50	7.69
ABC	64	0.75	8.75
ABC	64	1	9.51
ABC	128	0.24	7.82
ABC	128	0.47	10.04
ABC	128	0.71	11.92
ABC	128	0.86	12.71

Fig. 2: (Colour on-line) Absolute equilibrium kinetic-energy spectrum and magnetic energy spectrum during the linear regime of dynamo growth (obtained with a small random initial magnetic seed) with $k_0 = 40$ and $R_m = 20$ and resolution 128^3 (corresponding to $\zeta = 0.86$ in fig. 3(a)). $E_u(k)$ still remains in absolute equilibrium as in the initial state, while $E_b(k)$ has developed a tail and a dominant large-scale mode at $k = 1$. The dashed line in (a) represents the fit using eqs. (4) with $\alpha = 1.75 \times 10^6$ and $\beta = 4.15 \times 10^4$.

The critical R_m for dynamo dynamo action in this forced flow at two different resolutions is shown in table 1 ($R_m^c \sim 10$). These results were obtained at a moderate kinetic Reynolds number ($Re = 200$ and thus $P_m \sim .05$). First, they show that it can be realistic to model the scales of the flow larger than the forcing scale as if they were in absolute equilibrium. Indeed, compare the critical R_m of forced and AE computations with $k_0 = k_{\max} = N/3$. Second, velocity fluctuations do not increase much the dynamo threshold provided that the forcing is helical and that a wide scale separation is allowed. Indeed, compare the critical R_m of the two forced runs with the single-mode ABC runs (described below) with $k_0 = \zeta k_{\max} = \zeta N/3$.

Absolute equilibrium. – In the experimental context of liquid metals, a more "realistic" computation would require to further decrease the magnetic Prandtl number. However, a huge resolution would then be needed to perform a DNS. Indeed, when Re is increased, modes with wave numbers beyond the scale separation range (k_{box}–k_0) become populated by the turbulent cascade that takes place from forcing wave number k_0 down to dissipative wave number $k_d \sim k_0 Re^{3/4}$.

Note that the turbulent dynamo problem is already a very difficult one, even without a scale separation range. It was proposed to circumvent the difficulty of resolving the large range of scales by combining direct numerical simulations with Lagrangian-averaged model and large-eddy simulations [2].

In the present work we propose to focus instead on the problem with a large scale separation and to make use of the special structure of the energy spectrum in the scale separation range, that can be represented as a so-called absolute equilibrium. Indeed, as noted above when discussing fig. 1(b), $H(k)/E(k)$ vs. k^2 is almost linear up to $k = 20$ which is expected for AE (see eqs. (4) below).

Since the pioneering study of Lee (1952) [11] on the behavior of conservative systems with Fourier truncation at $k = k_{\max}$, the dynamics of the unforced spectrally truncated Euler equation is known to reach at large times an absolute equilibrium that is a statistically stationary Gaussian exact solution of the associated Liouville equation [12]. When the flow has a non-vanishing helicity, the absolute equilibria of the kinetic energy and helicity were obtained by Kraichnan [13] and explicitly read

$$E_u(k) = \frac{k^2}{\alpha} \frac{4\pi}{1 - \beta^2 k^2/\alpha^2}, \quad H(k) = \frac{k^4 \beta}{\alpha^2} \frac{8\pi}{1 - \beta^2 k^2/\alpha^2} \tag{4}$$

with α and β determined by the initial kinetic energy and helicity.

Note that if one intends to directly study the dynamo problem in the $P_m \to 0$ limit, it amounts to setting $\nu = 0$ and $f = 0$ in eq. (1). In this limit, the velocity initial data alone controls the flow on which the dynamo stability is investigated.

AE dynamo with scale separation at $P_m = 0$ vs. single-mode ABC dynamos at large P_m. – We now turn to the study of the ABC kinematic dynamo problem with zero forcing and zero viscosity. The initial ABC flow is at $k = k_0$ with small magnetic seed at $k = k_{\mathrm{box}}$. As the ABC flow is an exact but *unstable* solution of the Euler equation, the roundoff error grows rapidly and the flow settles into an absolute equilibrium as displayed in fig. 2(a). The steep rise of $E_u(k)$ at high k is related to the denominator of eqs. (4). Dynamos are clearly present in helical absolute equilibria with growing large-scale magnetic field as shown in fig. 2(b).

Figure 3(a) shows the computed growth rate of E_b for various R_m at resolution of 32^3, 64^3 and 128^3 with various values of $\zeta = k_0/k_{\max}$, where k_0 is the wave number of the ABC initial data used to generate the absolute equilibrium of the Euler equation. (Beside scale separation, ζ also controls the helicity $H = \langle \boldsymbol{u} \cdot \nabla \times \boldsymbol{u} \rangle = 2k_0 E_u$.)

Figure 3(b) shows the critical R_m at which the inception of dynamo action takes place. The increase in ζ is seen to result in a decrease in critical R_m. By inspection of
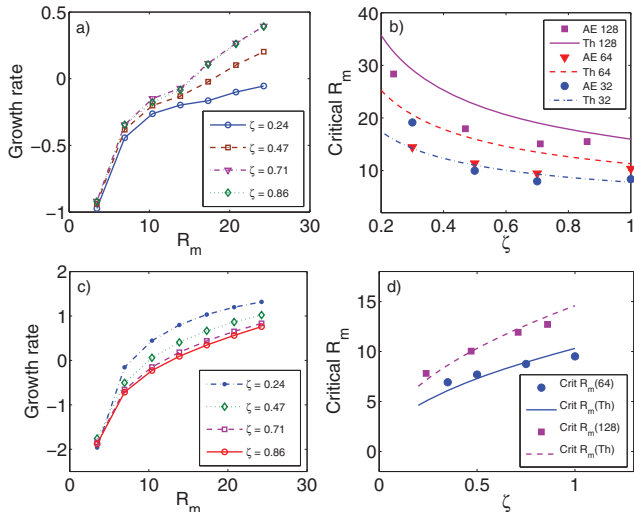
Fig. 3: (Colour on-line) Comparison of growth rates of magnetic energy E_b: (a) absolute equilibrium velocity field at resolution 128^3. (b) Critical R_m (determined by interpolation) together with theoretical scaling analysis at resolutions 32^3, 64^3 and 128^3. (c) Same as (a) but for single-mode ABC flow. (d) Same as (b) but for single-mode ABC flow and resolutions 64^3 and 128^3.

the magnetic energy spectrum, the wave number k_B of the growing dominant mode is found to be $k_{box} = 1$ (see fig. 2(b)).

Note that maximal-helicity ($\zeta = 1$) absolute equilibrium has critical R_m that is comparable with that of the forced ABC case (see table 1). Furthermore, 3D visualizations of the growing magnetic mode and the kinetic energy obtained for absolute equilibrium (fig. 4(a)) are very similar to those corresponding to the forced case (fig. 4(b)).

It is apparent in fig. 2(a) that some of the AE kinetic-energy spectra are rather well peaked at maximum wave number (as can be expected from eqs. (4)). This naturally leads us to study the problem of a single-mode ABC dynamo with scale separation. Note that the forcing will generate a single ABC mode at $k = k_0$ in the limit $Re \to 0$ or large P_m: the opposite limit to that studied with AE flows.

The scale separation dependence of the single-mode large P_m number ABC kinematic dynamo is presented in fig. 3. Figure 3(c) shows the computed growth rate of E_b for various R_m at resolution of 128^3 and at various values of $\zeta = k_0/k_{max}$. Contrary to the case of the AE flow, the single-mode ABC initial condition displays an opposite bifurcation trend. An increase in ζ corresponds to an increase in critical R_m.

Dependence of critical R_m on scale separation. –

Scaling of single-mode ABC dynamo. The scaling of the critical R_m with scale separation k_0/k_B can be understood by the following argument. The growth of a large-scale magnetic field is governed by the electromotive force (emf) term $\boldsymbol{u} \times \boldsymbol{b}$ in the induction equation (2). With a
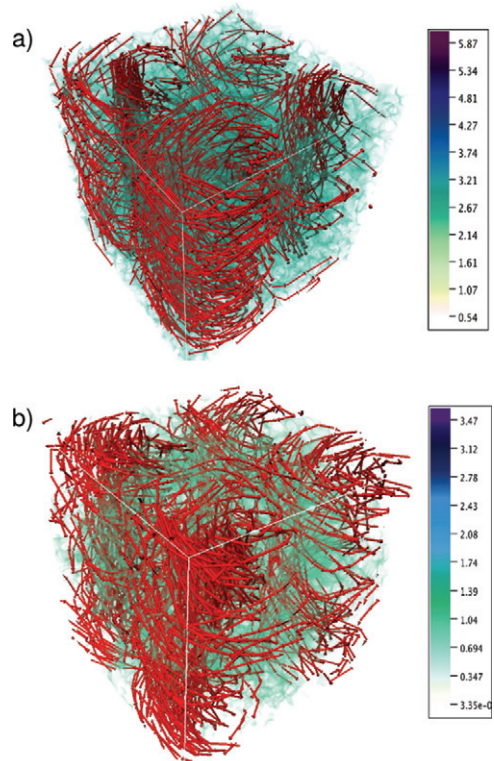
Fig. 4: (Colour on-line) Visualization of the growing magnetic field represented by arrows at a resolution of 128^3. (a) AE velocity, (b) forced ABC velocity. The 3D volume rendering corresponds to the kinetic energy of absolute equilibrium at maximum intensity.

small scale $\boldsymbol{u} = \boldsymbol{u}_{ABC}^{(k_0)}$, the magnetic field can be written as $\boldsymbol{b} = \boldsymbol{B}_0 + \boldsymbol{b}'$, where $\boldsymbol{B}_0$ is a large scale and $\boldsymbol{b}'$ a small scale. At first order in the small-scale magnetic Reynolds number $\boldsymbol{b}' = -(\eta\Delta)^{-1}\nabla \times (\boldsymbol{u} \times \boldsymbol{B}_0)$ and one finds that the average emf can be written as

$$\alpha \boldsymbol{B}_0 = \langle \boldsymbol{u} \times \boldsymbol{b}' \rangle = -\frac{\boldsymbol{u}^2}{\eta k_0} \boldsymbol{B}_0. \tag{5}$$

The resulting so-called α-effect evolution equation for $\boldsymbol{B}_0$ is

$$\partial_t \boldsymbol{B}_0 = \alpha \nabla \times \boldsymbol{B}_0 + \eta \Delta \boldsymbol{B}_0 \tag{6}$$

and implies criticality for $\eta_c = |\alpha|/k_B$, where k_B is the wave number corresponding to $\boldsymbol{B}_0$. Thus, the critical R_m is given by

$$R_m^c = \frac{\sqrt{2E_u}}{k_B \eta_c} = \sqrt{\frac{k_0}{k_B}}. \tag{7}$$

Note that this theoretical result is valid at first order in the small-scale Reynolds number in the limit of large scale separation k_0/k_B. With the moderate scale separation values used in the present work the scaling exponent of R_m^c becomes apparent but the prefactor needs a correction. The large-scale computations, with resolution larger than 1024^3, that are needed to check the convergence of the prefactor to 1 are left for a future study. Figure 3(d) shows the comparison of this scaling with the calculated

critical R_m from numerical computations (at three different resolutions of $32^3, 64^3, 128^3$) with an additional factor of 2.25. The square-root behavior is clearly visible and is due to the α-effect where the scale separation is more discernible in the case of large k_0.

Scaling of the AE dynamo.   Using first-order smoothing approximation, it has been shown [14] that

$$\alpha = -\frac{\eta}{3} \int \frac{k^2 H(\boldsymbol{k},\omega)}{\omega^2 + \eta^2 k^4} \mathrm{d}\boldsymbol{k} \mathrm{d}\omega, \tag{8}$$

where $H(\boldsymbol{k},\omega)$ denotes the Fourier transform of the spatiotemporal helicity fluctuations.

On dimensional grounds, the effective viscosity related to AE is given by $\sqrt{E_u}/k_{\max}$ and the velocity correlation time is given by $k_{\max}/\sqrt{E_u}k^2$. Thus, the effective integration range for ω in eq. (8) is limited to values smaller than $\sqrt{E_u}k^2/k_{\max}$. As $\omega/\eta k^2 \sim \sqrt{E_u}/\eta k_{\max} \ll 1$ at the dynamo threshold (in the limit of large scale separation) the integral over ω yields

$$\alpha \sim \frac{1}{\eta} \int \frac{H(k)}{k^2} \mathrm{d}k. \tag{9}$$

Equations (4) show that, for moderate values of $\beta^2 k^2/\alpha^2$, the absolute equilibrium helicity spectrum roughly scales as $H(k) \sim \gamma k^4$ and moreover the total helicity $H = \int_0^{k_{\max}} H(k)\mathrm{d}k$ has a value $H \approx k_0 E_u$. This results in an approximate expression for γ given by $\gamma \sim 5k_0 E_u/k_{\max}^5$. Thus, the magnitude of α for absolute equilibrium velocity field is approximately given by $\alpha^{\mathrm{AE}} \sim 5k_0 E_u/3\eta k_{\max}^2$. Similar to the case of ABC dynamo, the expression for the most unstable mode can be written as, $k_B = 5k_0 E_u/3k_{\max}^2 \eta^2$ which results in the expression for critical magnetic R_m given by

$$R_m^c = \frac{\sqrt{2E_u}}{k_B \eta_c} \approx \sqrt{\frac{6k_{\max}^2}{5k_B k_0}}. \tag{10}$$

Figure 3(b) shows the comparison of this scaling (with an additional prefactor of 2.25) with our AE numerical computations. It is visible that the trend persists up to a 128^3 resolution.

The beating mechanism explained above for ABC flow with a single mode acts on a wider scale for the AE spectrum since it possesses energy at varying length of the eddies. Thus, the interaction of high-energy small eddies in velocity results in the formation of tail-like feature in $E_b(k)$ as seen in fig. 2(b). It is also the interaction of these small scales that results in the growth of a large-scale magnetic field.

Now, in order to bring out the similarity between single-mode ABC and AE flow, we consider specific scenarios in both cases. From eqs. (4) it is visible that the spectrum becomes more pointed towards $k_{\max}$ for high initial helicity. This spectrum is in some sense similar to the single-mode ABC flow with k_0 close to $k_{\max}$. To wit, we compare the
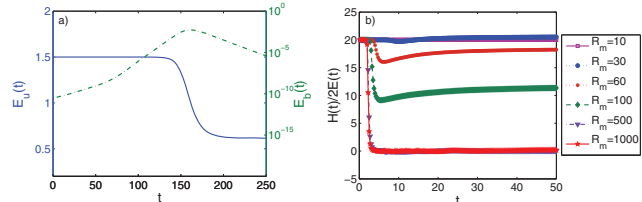
Fig. 5: (Colour on-line) (a) Evolution of kinetic and magnetic energy with time indicating saturation when $k_0 = 20$ at resolution 64^3. (b) Ratio of helicity to kinetic energy *vs.* time during the saturation and the decay of the magnetic field.

behavior of the dynamo generation due to both ABC flow and AE initial condition with maximum possible helicity at a given resolution. Figures 3(b) and (d) show that the critical R_m for both the scenarios are close to each other at high k_0 where ABC flow and AE behave equivalently in generating a dynamo. Strikingly, in eqs. (7) and (10), the corresponding analytical expressions for critical R_m, have similar proportional behavior only when $k_{\max} = k_0$ with equivalent α-effect as well.

Nonlinear saturation of the magnetic field for the AE dynamo. – The exponential growth of a magnetic field above the dynamo threshold first saturates because of the Lorentz-force back reaction on the flow. In a second stage, the magnetic field is observed to decay to zero exponentially in time (fig. 5(a)). This results from the absence of flow forcing (only a given initial amount of kinetic energy is present in the initial data). Although there is no viscous dissipation, the magnetic diffusivity alone is able to significantly dissipate the total energy (when the magnetic field has grown enough). Non-trivial effects are however found to take place in this framework.

Both H and E_u decrease in time and saturate to constant values in the long time limit. Figure 5(b) shows that the long-time saturation value of H/E_u strongly depends on R_m. For small supercriticality ($R_m \leq 30$) H/E_u is almost unchanged, whereas its saturation value decreases monotonously towards zero at larger R_m. The large R_m decrease of the saturation value is readily explained as follows. In the limit $R_m \to \infty$ there is no dissipation and magnetic absolute equilibrium can take place. There are 3 invariants: total energy, magnetic helicity and cross-helicity, that completely define the magnetic equilibrium [15]. As the initial values of magnetic helicity and cross-helicity are very small, it is easy to show (see eq. (25) in reference [15]) that such equilibration will destroy the kinetic helicity. It is remarkable that the saturation value of the relative kinetic helicity H/E_u behaves monotonously with respect to the distance to the dynamo threshold $R_m - R_m^c$ (see fig. 5(b)).

Conclusion. – Using the results of our study we can conclude by proposing a new configuration for a future dynamo experiment. The idea is to drive a sodium flow in a cubic meter of liquid sodium using a Roberts flow

forcing as in the Karlsruhe experiment but without constraining the flow in a periodic array of pipes. A Roberts flow forcing can be achieved using a square array of counterrotating vertical spindles, each of them fitted with several propellers. Both vertical and azimuthal flows are driven around each spindle, in a manner similar to a screw spindle pump. Both the vertical and azimuthal velocities change sign from one spindle to its neighbours. In contrast to the Karlsruhe experiment, a large-scale flow up to the size of the container, involving turbulent fluctuations, can develop in this device. From the hydrodynamic viewpoint, it will be of fundamental interest to characterize these hydrodynamic fluctuations and to check that their spectrum at wave numbers below the forcing scale do correspond to statistical equilibrium. To the best of our knowledge, the experimental study of turbulent spectra in this range has never been performed. The present study has shown that this type of flow involving both helical forcing and scale separation can provide an efficient way to reach a dynamo regime generated by a turbulent flow without geometrical constraints. This configuration can be an alternative to dynamo experiments using turbulent flows without scale separation [16–18] that have not displayed the dynamo effect so far, except when ferromagnetic impellers are used [19].

REFERENCES

[1] MOFFATT H. K., *Magnetic Field Generation in Electrically Conducting Fluids* (Cambridge University Press) 1978.
[2] PONTY Y., MININNI P. D., MONTGOMERY D. C., PINTON J.-F., POLITANO H. and POUQUET A., *Phys. Rev. Lett.*, **94** (2005) 164502.
[3] GISSINGER C., DORMY E. and FAUVE S., *Phys. Rev. Lett.*, **101** (2008) 144502.
[4] MININNI P. D. and MONTGOMERY D. C., *Phys. Rev. E*, **72** (2005) 056320.
[5] ISKAKOV A. B., SCHEKOCHIHIN A. A., COWLEY S. C., MCWILLIAMS J. C. and PROCTOR M. R. E., *Phys. Rev. Lett.*, **98** (2007) 208501.
[6] MININNI P. D., *Phys. Rev. E*, **76** (2007) 026316.
[7] FRISCH U., *Fully developed turbulence and intermittency*, in *Proceedings of Turbulence and Predictability in Geophysical Fluid Dynamics and Climate Dynamics*, edited by GIL M., BENZI R. and PARISI G. (Elsevier, Amsterdam; North-Holland) 1985, pp. 71–88.
[8] STIEGLITZ R. and MÜLLER U., *Phys. Fluids*, **13** (2001) 561.
[9] MININNI P. D., ROSENBERG D., REDDY R. and POUQUET A., *Parallel Comput.*, **37** (2011) 316.
[10] GOTTLIEB D. and ORSZAG S. A., *Numerical Analysis of Spectral Methods* (SIAM, Philadelphia) 1977.
[11] LEE T., *Q. Appl. Math.*, **10** (1952) 69.
[12] ORSZAG S., *J. Fluid Mech.*, **41** (1970).
[13] KRAICHNAN R., *J. Fluid Mech.*, **59** (1973) 745.
[14] MOFFATT H. and PROCTOR M., *Geophys. Astrophys. Fluid Dyn.*, **21** (1982) 265.
[15] FRISCH U., POUQUET A., LÉORAT J. and MAZURE A., *J. Fluid Mech.*, **68** (1975) 769.
[16] PEFFLEY N. L., CAWTHORNE A. B. and LATHROP D. P., *Phys. Rev. E*, **61** (2000) 5287.
[17] SPENCE E. J., NORNBERG M. D., JACOBSON C. M., PARADA C. A., TAYLOR N. Z., KENDRICK R. D. and FOREST C. B., *Phys. Rev. Lett.*, **98** (2007) 164503.
[18] COLGATE S. A., BECKLEY H., SI J., MARTINIC J., WESTPFAHL D., SLUTZ J., WESTROM C., KLEIN B., SCHENDEL P., SCHARLE C., MCKINNEY T., GINANNI R., BENTLEY I., MICKEY T., FERREL R., LI H., PARIEV V. and FINN J., *Phys. Rev. Lett.*, **106** (2011) 175003.
[19] MONCHAUX R., BERHANU M., BOURGOIN M., MOULIN M., ODIER P., PINTON J.-F., VOLK R., FAUVE S., MORDANT N., PÉTRÉLIS F., CHIFFAUDEL A., DAVIAUD F., DUBRULLE B., GASQUET C., MARIÉ L. and RAVELET F., *Phys. Rev. Lett.*, **98** (2007) 044502.